Recombinant Expression and Enzymatic Characterization of PttCel9A, a KOR Homologue from Populus tremula x tremuloides †

ARTICLE *in* BIOCHEMISTRY · SEPTEMBER 2004

Impact Factor: 3.02 · DOI: 10.1021/bi049453x · Source: PubMed

8 AUTHORS, INCLUDING:

Weilin Zhou

25 PUBLICATIONS **1,093** CITATIONS

SEE PROFILE

David Wilson

Cornell University

245 PUBLICATIONS **8,412** CITATIONS

SEE PROFILE

Recombinant Expression and Enzymatic Characterization of PttCel9A, a KOR Homologue from *Populus tremula x tremuloides*†

Emma R. Master,‡ Ulla J. Rudsander,‡ Weilin Zhou,§ Hongbin Henriksson,‡ Christina Divne,‡ Stuart Denman,‡ David B. Wilson,§ and Tuula T. Teeri*,‡

Department of Biotechnology, Royal Institute of Technology (KTH), AlbaNova University Center, Stockholm, Sweden, and Department of Molecular Biology and Genetics, Cornell University, 458 Biotechnology Building, Ithaca, New York 14853-2703

Received March 19, 2004; Revised Manuscript Received May 12, 2004

ABSTRACT: PttCel9A is a membrane-bound, family 9 glycosyl hydrolase from *Populus tremula x tremuloides* that is upregulated during secondary cell wall synthesis. The catalytic domain of PttCel9A, Δ_{1-105}PttCel9A, was purified, and its activity was compared to TfCel9A and TfCel9B from *Thermobifida fusca*. Since aromatic amino acids involved in substrate binding at subsites −4, −3, and −2 are missing in PttCel9A, the activity of TfCel9A mutant enzymes W256S, W209A, and W313G was also investigated. Δ_{1-105}PttCel9A hydrolyzed a comparatively narrow range of polymeric substrates, and the preferred substrate was (carboxymethyl)cellulose 4M. Moreover, Δ_{1-105}PttCel9A did not hydrolyze oligosaccharides shorter than cellopentaose, whereas TfCel9A and TfCel9B hydrolyzed cellotetraose and cellotriose, respectively. These data suggest that the preferred substrates of PttCel9A are long, low-substituted, soluble cellulosic polymers. At 30 °C and pH 6.0, the k_{cat} for cellohexaose of Δ_{1-105}PttCel9A, TfCel9A, and TfCel9B were 0.023 ± 0.001, 16.9 ± 2.0, and 1.3 ± 0.2, respectively. The catalytic efficiency (k_{cat}/K_m) of TfCel9B was 39% of that of TfCel9A, whereas the catalytic efficiency of Δ_{1-105}PttCel9A was 0.04% of that of TfCel9A. Removing tryptophan residues at subsites −4, −3, and −2 decreased the efficiency of cellohexaose hydrolysis by TfCel9A. Mutation of W313 to G had the most drastic effect, producing a mutant enzyme with 1% of the catalytic efficiency of TfCel9A. The apparent narrow substrate range and catalytic efficiency of PttCel9A are correlated with a lack of aromatic amino acids in the substrate binding cleft and may be necessary to prevent excessive hydrolysis of cell wall polysaccharides during cell wall formation.

The secondary cell wall of wood fibers consists of a complex matrix of polymers, including polysaccharides, proteins, and phenolic compounds. Cellulose is a major component of plant cell walls, and its organization in secondary cell walls affects the property of wood fibers. Since cellulose synthesis and deposition result from coordinated activities of enzymes, biotechnological methods are an attractive option for industrial fiber engineering.

To identify genes that could be targeted for fiber engineering, expression profiling was previously performed on an EST database of 3000 cambial sequences assembled from the hybrid aspen, *Populus tremula x tremuloides* Mich. (http://poppel.fysbot.umu.se) (*1*, *2*). Several genes that encode carbohydrate-active enzymes and are upregulated during xylogenesis were identified, including ten that encode putative cellulose synthases (CesA) (*3*) and at least two that encode family 9 glycosyl hydrolases (GH9) (*4*). One of the putative cellulases, PttCel9A, is upregulated during secondary cell wall formation, which coincides with a period of intensive cellulose synthesis (*4*). The secreted GH9 enzymes from *Populus calli*, PopCel1 and PopCel2, have been implicated in cell wall loosening during cell expansion (*5*, *6*). However, cell wall loosening is probably not the primary function of PttCel9A, which is membrane-anchored and upregulated after cell expansion. Accordingly, PttCel9A may function in cellulose synthesis or cell wall assembly, making it an interesting target for fiber engineering.

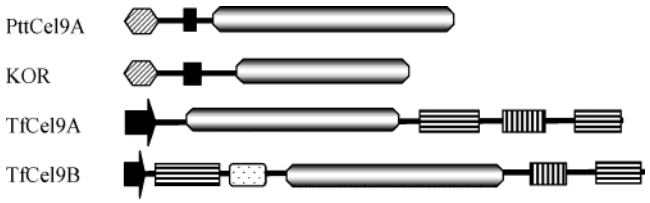

FIGURE 1: Comparison of the PttCel9A modular structure and sequence with selected family 9 glycosyl hydrolases. Schematic representation of enzyme domains: signal sequence (black arrow), cytoplasmic domain (striped hexagon), transmembrane anchor (black box), catalytic domain (gray-white hexagon), fibronectin-like module (vertical stripes), cellulose-binding module (horizontal stripes), Ig-like module (dots).

PttCel9A contains an N-terminal cytoplasmic tail followed by a membrane spanning region and a C-terminal catalytic domain that belongs to family GH9 (CAZy, http://afmb.cnrs-mrs.fr/CAZY/index.html) (Figure 1). Moreover, PttCel9A shares over 82% sequence identity with the *Arabidopsis*

† This work was financed by grants from the Knut and Alice Wallenberg Foundation and the European Union, Project QLK5-CT2001-00443.

* Corresponding author. Phone: +46-8-5537 8381. Fax: +46-8-5537 8483. E-mail: tuula@biotech.kth.se.

‡ AlbaNova University Center.

§ Cornell University.

10.1021/bi049453x CCC: $27.50
Published on Web 07/15/2004

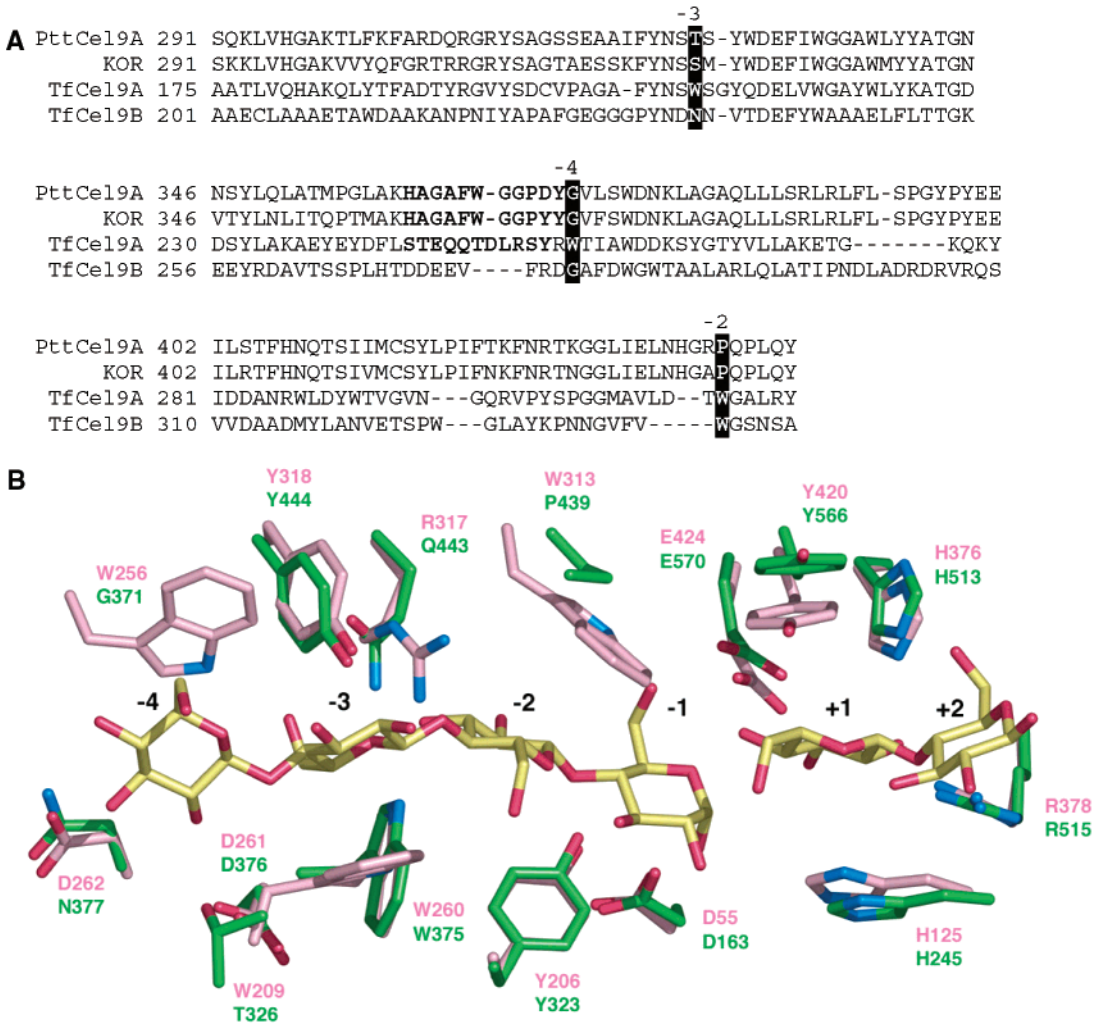

FIGURE 2: (A) Sequence alignment indicating the positions of the blocking loop (bold type) and substrate binding subsites −4, −3, and −2 (highlighted). Numbering is from full-length sequences of PttCel9A and KOR and the catalytic domains of TfCel9A and TfCel9B. (B) Superposition of the active site in the experimentally determined structure of TfCel9A (violet) and that of the modeled PttCel9A (green). Only residues in TfCel9A that interact through hydrogen bonds or Trp stacking are shown. The TfCel9A structure is in complex with cellotetraose (subsites −4 to −1) and cellobiose molecules (subsites +1 and +2). The reducing end of the binding cleft is to the right, and the nonreducing end is to the left in the picture. The picture was made with the program PyMOL (*39*).

thaliana enzyme KOR, which was identified in korrigan, a mutant characterized by irregular cell surfaces, shape, and reduced cellulose content (*7*). Additional mutations in KOR have since been isolated and consistently generate plants with reduced cellulose content and abnormal cell shape, suggesting a role for KOR in cellulose synthesis or modification (*8*, *9*).

In *A. thaliana*, KOR is expressed in developing xylem but might not form part of the cellulose synthase complex (*10*). KOR and KOR homologues are identified in various subcellular localizations, including the phragmoplast (*11*), Golgi vesicles (*12*), plasma membrane, and intracellular vesicles (*13*). Although these data are somewhat conflicting, it is conceivable that KOR and homologous enzymes are shuttled to different cellular compartments depending on cell type and developmental phase (*14*). Data from recombinantly expressed Cel16, a KOR orthologue from *Brassica napus*, show that this enzyme hydrolyzes soluble, low-substituted cellulosic substrates and not hemicellulosic compounds (*15*). Since cellulose is synthesized and modified at the plasma membrane, these data support the proposal that KOR and homologous enzymes function in the cell wall. Notably, the participation of soluble and membrane-bound endoglucanases in cellulose synthesis or assembly has already been described for several bacteria (*16*−*18*).

To further elucidate the role of membrane-bound endoglucanases in plants, we report the recombinant expression and in vitro characterization of the catalytic domain of PttCel9A. A comparison of PttCel9A and Cel16, which share over 82% sequence identity, was performed to test whether the relatively narrow substrate range of Cel16 is characteristic of plant membrane-bound endoglucanases. The activity of PttCel9A is also compared to two, well-characterized GH9 enzymes from *Thermobifida fusca*, TfCel9A and TfCel9B (*19*, *20*). TfCel9A shares 35% sequence identity with PttCel9A and is a processive endoglucanase, whereas TfCel9B shares less than 10% sequence identity with PttCel9A and is a true endoglucanase. The structure of TfCel9A is known (*19*) and was previously used to generate a model structure of PttCel9A (*4*). Like TfCel9A, PttCel9A contains a loop blocking the nonreducing end of the substrate binding cleft (Figure 2A). However, PttCel9A lacks tryptophan residues at positions corresponding to 256, 209, and 313 in TfCel9A, which are involved in substrate binding at subsites −4, −3, and −2, respectively (*4*, *19*) (Figure 2B).

Since aromatic amino acids are commonly involved in substrate binding by cellulases (*21*, *22*), the effect of the amino acid substitutions, W256A, W209S and W313G, on TfCel9A activity was investigated. This comparison shows how the absence of aromatic residues at substrate binding sites contributes to PttCel9A activity. As a result, these data provide the basis for predicting modifications in PttCel9A that could lead to new fiber compositions and properties and represent the first detailed kinetic analysis of a plant, membrane-anchored endoglucanase.

EXPERIMENTAL PROCEDURES

General. Buffers were prepared using water purified on a Milli-Q system (Millipore) with a resistivity ≥18.2 MΩ• cm. Nucleotide sequences were determined by AmpliTaq FS DyeDeoxy terminator cycle sequencing chemistry (PE Biosystems). Sodium dodecyl sulfate−polyacrylamide gel electrophoresis (SDS−PAGE) analyses were performed using 10% resolving gels and marker proteins (LMW calibration kit) from Amersham Biosciences. Proteins were visualized by Coomassie Blue staining (*23*) or silver staining (*24*). Protein concentration was determined using the Bradford assay and bovine serum albumin as the standard (*23*). Spectrophotometric measurements were performed using a Cary 50 UV−vis spectrophotometer (Varian Instruments).

Enzyme Substrates. (Carboxymethyl)cellulose, low viscosity (CMC),[1] cellobiose, and xylan from birchwood were purchased from Sigma. (Carboxymethyl)cellulose 4M [CMC-(4M)], lichenan (Icelandic moss), Konjac glucomannan, and xyloglucan from tamarind seed (high viscosity) were purchased from Megazyme. (Hydroxyethyl)cellulose (HEC), Avicel PH-101 (microcrystalline cellulose), and cellotetraose were purchased from Fluka. Cellohexaose was purchased from Seikagaku. Cellotriose, cellopentaose, 4-methylumbelliferyl cello-oligosaccharides (MeUmbGs) $MeUmb_2$, $MeUmb_3$, $MeUmb_4$, $MeUmb_5$, and $MeUmb_6$ were kind gifts from Prof. M. Claeyssens (Rijksuniversiteit, Gent, Belgium). Phosphoric acid swollen cellulose (PASC) was prepared from Avicel by adding 150 mL of ice-cold, 85% orthophosphoric acid to 5 g of Avicel followed by continuous stirring for 1 h in an ice bath. Ice-cold acetone was then added to the mixture with continued stirring, and the mixture was transferred to a glass filter funnel and then washed with 3 × 100 mL of ice-cold acetone followed by 3 × 100 mL washes with Milli-Q water. Finally, PASC was suspended in 300 mL of Milli-Q water, homogenized in a blender, and stored at 4 °C.

Expression of Recombinant PttCel9A. A full-length cDNA corresponding to PttCel9A was previously isolated and cloned (*4*). The region of the *PttCel9A* gene that corresponds to the catalytic domain of PttCel9A was amplified by PCR using a proofreading DNA polymerase (Pfu from Stratagene) and the following forward and reverse primers, respectively: 5′-CATCATCATCATCATCATCCAGCTGATAACTACACTCTTGCG-3′ and 5′-TCATGGTTTCCAAGGTGCTGG-3′. To facilitate subsequent purification steps, the forward primer introduced a His-tag (underlined) at the N-terminus of the expressed protein. The amplified fragment was cloned in the *Sna*BI site of the pPIC9 *Pichia pastoris* expression vector (Invitrogen), generating pPIC9-Δ_{1-105}-PttCel9A. Thus, the coding sequence of Δ_{1-105}PttCel9A was fused in frame with an upstream vector sequence that encodes the signal sequence of the *Saccharomyces cerevisiae* α-factor. Following sequencing, pPIC9-Δ_{1-105}PttCel9A was linearized with *Sac*I and then transformed into *P. pastoris* GS115 by electroporation following the manufacturer's instructions (Invitrogen, *Pichia* Expression Version M).

Production and Purification of Recombinant PttCel9A. Transformants were selected on methanol medium lacking histidine and then screened for expression of Δ_{1-105}PttCel9A by immuno-colony blot using nitrocellulose membranes (0.45 μm, Bio-Rad), PttCe9A peptide antibodies, horseradish-linked anti-rabbit IgG, and the ECL Western blot analysis system (Amersham Biosciences). The presence of the *PttCel9A* gene fragment in positive clones was confirmed by direct PCR amplification.

Positive transformants were added to 5 mL of buffered glycerol-complex medium (BMGY) [1% yeast extract, 2% peptone, 100 mM potassium phosphate (pH 6.0), 1.34% YNB, (4×10^{-5})% biotin, 1% glycerol] in 50 mL conical tubes and then incubated overnight at 30 °C with continuous rotary shaking at 200 rpm. Cells were harvested by centrifugation and then suspended in 2 × 1 L of buffered methanol-complex medium (BMMY) [1% yeast extract, 2% peptone, 100 mM potassium phosphate (pH 6.0), 1.34% YNB, 4×10^{-5} % biotin, 0.5% methanol] in two 5 L flasks to $D_{600} \approx 0.5$. Cultures were incubated for 3 days at 22 °C with continuous rotary shaking at 180 rpm. Methanol was added to a final concentration of 0.5% every 24 h. Supernatant from the methanol-induced cultivations was filtered through a 0.45 μm Versapor membrane (Pall Corp.) and concentrated by ultrafiltration at 4 °C. The concentrated culture medium was replaced by 20 mM phosphate buffer including 0.5 M NaCl (pH 7.4) by gel filtration with Sephadex gel (Pharmacia Biotech) and then applied to chelating Sepharose Fast Flow gel (Pharmacia Biotech) charged with Co^{2+} and packed in a XK16 column (Amersham Biosciences). Proteins were eluted by a linear gradient of 0−0.5 M imidazole in 20 mM phosphate buffer including 0.5 M NaCl (pH 7.4) over 5 column volumes. Fractions (1 mL) were collected at a flow rate of 1 mL min^{-1}. Fractions eluted with imidazole were pooled, the buffer was replaced by 50 mM sodium acetate (pH 5.5), and the sample was applied to a Resource S 1 mL column (Amersham Biosciences). Δ_{1-105}PttCel9A was eluted by a linear gradient of 0−1 M NaCl in 50 mM sodium acetate (pH 5.5) over 20 column volumes. Fractions (0.5 mL) were collected at a flow rate of 2 mL min^{-1}. All chromatographic steps were performed at room temperature, and fractions were collected at 4 °C.

The identity of the purified protein was confirmed by immunoblot using 2 μg of purified protein and a peptide specific antibody and by mass spectrophotometric analysis of tryptic peptides. The tryptic fragments were generated by incubating a gel fragment containing Δ_{1-105}PttCel9A that was cut from a 10% SDS−PAGE gel with approximately 30 ng of sequencing grade trypsin (Roche) overnight at room temperature (*25*, *26*). Tryptic peptides were extracted from

[1] Abbreviations: CMC, (carboxymethyl)cellulose; CMC(4M), (carboxymethyl)cellulose 4M; HEC, (hydroxyethyl)cellulose; PASC, phosphoric acid swollen cellulose; PCR, polymerase chain reaction; YNB, yeast nitrogen base; *D*, attenuance; MS, mass spectrometry; LMW, low molecular weight; TOF, time of flight; Q-Tof, hybrid quadrupole-orthogonal TOF.

the gel band and analyzed by a Q-Tof II mass spectrometer fitted with a nano-Z spray source (Waters Corp., Micromass MS Technologies, Manchester, U.K.). The instrument was operated at a resolution of over 10000, full width at half-maximum. Mass calibration was obtained over the *m*/*z* range 50−2000 using 1.5 g L^{-1} NaI in 50% 2-propanol. The extracted peptides were desalted to 50% acetonitrile containing 0.1% formic acid using C18ZipTip units (Millipore) according to the manufacturer's instructions and introduced into the mass spectrometer by infusion through the nano-Z spray source (syringe pump, 200 nL min^{-1}, source voltage 3.3 kV). Tof-MS data of the peptide mixtures were acquired over the *m*/*z* range 250−2000, and Tof-MS/MS data of the individual peptides were acquired over the mass range *m*/*z* 50−2000. The Maximum Entropy 3 algorithm was used to obtain a deconvoluted spectrum for each precursor ion from the MS/MS fragmentation, and de novo sequencing was performed using the MassLynx Software's PepSeq (Waters Corp., Micromass MS Technologies, Manchester, U.K.) to achieve the peptide sequence tags.

Site-Directed Mutagenesis, Expression, and Purification of TfCel9A68. Plasmid pJE2, encoding the *T. fusca* Cel6A signal sequence (MRMSPRPLRALLGAAAAALVSAAALAFPSQAA) followed by the mature Cel9A gene encoding the catalytic domain and cellulose binding module IIIc from pSZ46 (*27*) (E47 to G659, 613 amino acids) in the pET-26b+ vector (Novagen), was used as the template for mutagenesis. Site-directed mutagenesis was undertaken using the QuikChange site-directed mutagenesis methods (Stratagene). The primers used to introduce the mutations (underlined) were as follows: W209S, 5′-GCGTTCTACAACTCCTCGTCGGGCTACCAG-3′ (forward) and 5′-CTGGTAGCCCGACGAGGAGTTGTAGAACGC-3′ (reverse); W256A, 5′-GCTACCGGGCGACCATCGCCTGGGATGACAAGTCCTACGG-3′ (forward) and 5′-CCGTAGGACTTGTCATCCCAGGCGATGGTCGCCCGGTAGC-3′ (reverse); W313G, 5′-GCTCGACACCGGCGGGGCCCTGCGCTACGCCG-3′ (forward) and 5′-CGGCGTAGCGCAGGGCCCCGCCGGTGTCGAGC-3′ (reverse). The PCR product was transformed into *Escherichia coli* DH5α, and plasmid minipreps of individual transformants were screened by restriction enzyme digestion for the added or removed site. All mutations were verified by nucleotide sequencing using appropriate primers. Sequence-confirmed plasmid DNA was transformed into *E. coli* BL21-gold(DE3) (Stratagene) for expression. The *E. coli* BL21-gold(DE3) strains were grown at 37 °C overnight in 100 mL of LB with 60 μg mL^{-1} kanamycin. Thirty milliliters of this culture was transferred to each liter of M9 medium containing 0.5% glucose and 60 μg mL^{-1} kanamycin. After growth at 30 °C for about 5 h to $D_{600} \approx 0.8$, isopropyl thio-β-D-galactoside was added to the culture to 0.8 mM and growth continued at 30 °C for 16 h. Wild-type and mutant proteins were purified from the culture supernatants by a published procedure (*27*). Enzyme purity was assessed on SDS−PAGE gels.

Homology Modeling. The homology model previously reported (*4*) was refined by superimposing the deposited coordinates for the bacterial family 9 members TfCel9A (PDB accession number 4TF4), *Clostridium thermocellum* Cel9A (CtCel9A; PDB accession number 1CLC), *Clostridium cellulolyticum* Cel9M (CcCel9M; PDB accession number 1IA6), and *C. cellulolyticum* Cel9G (CcCel9G; PDB accession number 1K72) and then manually adding the amino acid sequence of PttCel9A to the alignment (data not shown). Guided by the structure-based sequence alignment, the sequence of the TfCel9A model was mutated in silico using the mutate commands in the program O (*28*) according to the amino acid sequence of PttCel9A. For each mutated amino acid, the side chain rotamer was chosen to agree as closely as possible with that of the original residue in the crystal structure (lego_side chain command in O). Neighboring atomic contacts were monitored by eye to optimize possible hydrogen-bonding, polar, electrostatic, and hydrophobic interactions and to avoid nonfavorable van der Waals interactions. For amino acid side chains on the surface, the most commonly observed rotamer was chosen for each type of amino acid. Insertions were built manually and optimized with the lego_loop command in O, followed by regularization of the coordinates in O (refi commands).

In the PttCel9A sequence, six cysteine residues that are not present in the template molecules were identified. The observation that most of these Cys residues appear in loop insertions indicated strongly that they participate in loop-stabilizing disulfide pairing. On the basis of this assumption, two loop regions in the poplar enzyme, which displayed no sequence similarity to the template molecules, were built de novo. Although the precise conformation of the individual loops is not determined in detail by the presence of the disulfide bonds, the degree of conformational freedom would be significantly reduced by the restraining S−S bonds. The two loop-stabilizing disulfide bonds are positioned in either of two nonconserved loop segments: at the end of the cellulose binding cleft where the reducing end of a cellulose chain is bound in TfCel9A and at the opposite end of the binding cleft where the nonreducing end is bound. The geometry of the homology model was relieved of unfavorable stereochemical strain by performing energy minimization with the program CNS (*29*).

Enzyme Activity with Polymeric Substrates. The standard activity assay was performed at 30 °C in 50 mM phosphate buffer (pH 6.0) containing 30 mM $CaCl_2$. Polymeric substrate concentrations varied from 0.01% (w/v) to 5% (w/v). Reactions were initiated by adding enzyme (10 ng μL^{-1}) and were incubated overnight. For Avicel and PASC, the reaction mixtures were incubated with gentle shaking. Initial rates of CMC(4M) hydrolysis were determined from nine time points over 15 min. Reactions were terminated and analyzed using the disodium 2,2′-bicinchoninate (BCA) assay for reducing sugars (*30*).

Enzyme Activity with Cello-oligosaccharides and 4-Methylumbelliferyl Cello-oligosaccharides (MeUmbGs). The activities of enzymes with cello-oligosaccharides from cellobiose (G2) to cellohexaose (G6) and MeUmbGs from $MeUmbG_2$ to $MeUmbG_6$ were tested using the standard activity assay with 250 μM of each oligosaccharide. Reactions were initiated by adding enzyme (10 ng μL^{-1}) and incubated overnight. Reactions were terminated by adding sodium hydroxide to 60 mM. The products of enzymatic hydrolysis were analyzed by thin-layer chromatography using a 3:1 ratio of acetonitrile and water and by high performance anion-exchange chromatography with a pulsed amperometric detector (HPAEC-PAD, Waters 2410) using a Waters 600S Controller pump and a CarboPac PA-100 column (Dionex). The eluents were 60 mM sodium hydroxide (eluent A) and

60 mM sodium hydroxide with 200 mM sodium acetate (eluent B). Elution was performed at a constant flow rate of 0.8 mL min^{-1} at room temperature using a linear gradient from 0% to 95% of eluent B. The injection volume was 10 μL in each case. The reaction products were identified and quantified relative to known standards.

Effect of Divalent Metal Cations. The effect of divalent metal cations on the activity of Δ_{1-105}PttCel9A was determined using the standard assay with CMC(4M) (0.1% w/v) as substrate and 5−60 mM $CaCl_2$, $MgCl_2$, or $ZnCl_2$. Reactions were initiated by adding enzyme (10 ng μL^{-1}) and incubated for 10 min. Reactions were terminated and analyzed as described above.

pH Profile. The effect of pH on the activity of Δ_{1-105}-PttCel9A was determined using the standard assay with CMC(4M) (0.1% w/v) as substrate and 100 mM phosphate solution, pH 3.0−11. Reactions were initiated by adding enzyme (10 ng μL^{-1}) and progressed for 10 min. Reactions were terminated and analyzed as described above.

Kinetic Measurements. Kinetic parameters were determined using the standard activity assay with oligosaccharide concentrations from 25 μM to 5 mM. Reactions were initiated by adding enzyme (0.5 ng μL^{-1} TfCel9A, TfCel9B, W209S, or W256A; 10 ng μL^{-1} W313G; 100 ng μL^{-1} PttCel9A) and incubated for up to 5 min. Reactions were terminated by adding sodium hydroxide to 60 mM. Hydrolysis activity was followed over a time course including six time points to confirm that initial rates were measured. The products from enzymatic hydrolysis were analyzed by HPAEC-PAD using a CarboPac PA-100 column (Dionex) as described above. The injection volume was 10 μL in each case, and the reaction products were identified and quantified relative to known standards. Kinetic constants were calculated from a Lineweaver−Burk plot.

Protein Deglycosylation. Deglycosylation of Δ_{1-105}PttCel9A by endoglycosidase H (Endo H, Roche) was performed for up to 2 h at 22 °C using 5 milliunits of Endo H per 20 μg of protein. Deglycosylation of Δ_{1-105}PttCel9A by protein *N*-glycosidase F (PNGase F) was performed under denaturing conditions according to the manufacturer's instructions (*N*-glycosidase F deglycosylation kit; Boehringer Mannheim).

RESULTS

Expression and Purification of Δ_{1-105}PttCel9A in P. pastoris. Of approximately 100 *P. pastoris* transformants that were screened by colony blotting, 3 expressed detectable levels of Δ_{1-105}PttCel9A. Maximal expression of Δ_{1-105}-PttCel9A in liquid medium with methanol was reached after 3 days at 22 °C. Therefore, 1 L cultivations were induced with methanol every 24 h for 3 days. To enable binding of Δ_{1-105}PttCel9A to the chelating Sepharose column, media in the concentrated supernatant was replaced by 20 mM Na_2HPO_4 (pH 7.4) containing 0.5 M NaCl. The best purification was achieved using chelating Sepharose charged with Co^{2+}, rather than Cu^{2+}or Ni^{2+}, and Δ_{1-105}PttCel9A eluted in approximately 125 mM imidazole. Δ_{1-105}PttCel9A was further purified and concentrated on a 1 mL Resource S column, where it eluted at 300 mM NaCl. The activity of Δ_{1-105}PttCel9A was followed during the purification by performing a standard activity assay with CMC(4M) (Table 1).

Table 1: Purification of Δ_{1-105}PttCel9A from *P. pastoris* Culture Medium

step	protein (mg)	activity[a] (units)	specific activity (units/mg)	yield (%)	purification (*x*-fold)
supernatant	64	88	1.4	100	1
chelating Co^{2+}	5.8	46	7.9	52	5.7
Resource S	2.2	42	18.8	47	13.7

[a] One unit of activity is defined by μmol of reducing ends released after 1 h incubation of the sample with CMC(4M) at 30 °C.

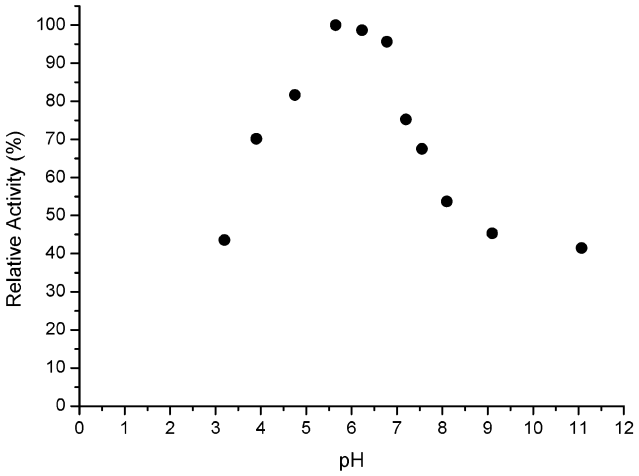

FIGURE 3: Effect of pH on hydrolysis of CMC(4M) by Δ_{1-105}-PttCel9A.

Analysis of purified Δ_{1-105}PttCel9A by gel electrophoresis revealed a band with an apparent molecular mass of 66 kDa and a diffuse band larger than 99 kDa. Upon deglycosylation with PNGase F, only a single band with an apparent molecular mass of 58 kDa, the theoretical molecular mass of the expressed protein, was observed. There are eight possible sites for N-glycosylation in Δ_{1-105}PttCel9A, and this result indicates that Δ_{1-105}PttCel9A expressed in *P. pastoris* is highly glycosylated. Deglycosylation of the recombinantly expressed *B. napus* endoglucanase, Cel16, resulted in the loss of over 90% of enzyme activity (*15*), while up to 80% of the activity of Δ_{1-105}PttCel9A was lost after deglycosylation with Endo H. The apparent molecular masses of several native, membrane-bound, plant endoglucanases exceed the theoretical molecular mass of the enzyme (*10*−*12*, *15*), indicating that these enzymes are posttranslationally modified in vivo, possibly via N-linked glycosylation.

The identity of the purified protein was confirmed by mass spectrometric analysis of tryptic peptides produced from an in-gel trypsin digest of the purified protein. This analysis produced five unique peptide sequences (tryptic fragments: T9, T11, T25, T32−33, and T44) that averaged 12 amino acids in length.

Effect of pH and Divalent Cations on Δ_{1-105}PttCel9A Activity. Hydrolysis of CMC(4M) by Δ_{1-105}PttCel9A was optimal between pH 5.5 and pH 6.0 (Figure 3). Thus, Δ_{1-105}PttCel9A appears to be more stable at low pH than the *B. napus* enzyme Cel16, which loses more than 60% of its activity from pH 6.0 to pH 5.5 (*15*). However, incubating PttCel9A below pH 4 or above pH 6.5 for 5 min prior to an activity assay greatly diminished hydrolysis of CMC(4M). Similar to Cel16, the activity of Δ_{1-105}PttCel9A was enhanced by increasing concentrations of $CaCl_2$, up to 30

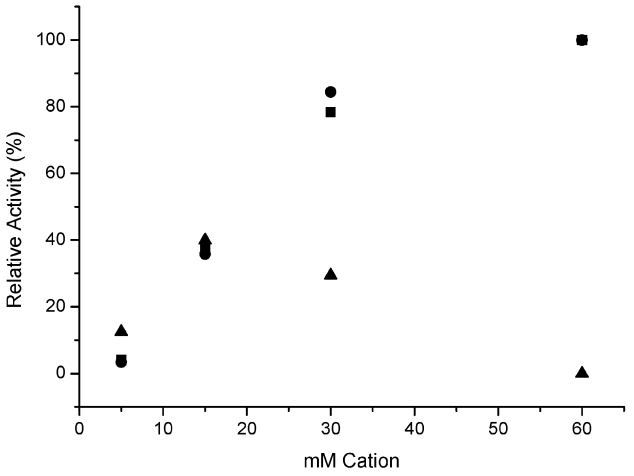

FIGURE 4: Effect of increasing concentrations of $CaCl_2$ (●), $MgCl_2$ (■), and $ZnCl_2$ (▲) on hydrolysis of CMC(4M) by Δ_{1-105}PttCel9A.

mM, and was inhibited by $ZnCl_2$ above 30 mM (Figure 4). The effect of Ca^{2+} ions on the activity of Δ_{1-105}PttCel9A is consistent with previous modeling studies that show that residues coordinating a Ca^{2+} ion in the bacterial endoglucanase, TfCel9A, are strictly conserved in Δ_{1-105}PttCel9A (*4*).

Activity with Polymeric Substrates. Δ_{1-105}PttCel9A had a narrower range of activity on polymeric substrates than TfCel9A and TfCel9B (Figure 5). Δ_{1-105}PttCel9A hydrolyzed CMC(4M), CMC, and PASC, although it showed a marked preference for CMC(4M). The number of side chains per 10 residues of the β-1,4-glucose backbone of CMC(4M), CMC, HEC, and xyloglucan are approximately 4, 8, 25, and 8, respectively. Thus, the difference in activity of Δ_{1-105}-PttCel9A with these compounds indicates that PttCel9A prefers substrates with a low degree of substitution. Avicel and PASC are also β-1,4-glucans but differ in their degree of crystallinity. Lichenan is unbranched and contains two β-1,4-glucose linkages for every β-1,3-glucose linkage. Low activity of Δ_{1-105}PttCel9A on lichenan suggests that more than three β-1,4-linked glucose units are required to efficiently bind in the substrate binding cleft of this enzyme. Inefficient substrate binding also would explain the low activity of Δ_{1-105}PttCel9A on glucomannan, since β-1,4-linked glycosyl units in this substrate are 40% glucose and 60% mannan. TfCel9A and TfCel9B had similar activity on crystalline cellulose; however, TfCel9B hydrolyzed lichenan and substituted β-1,4-glucans more efficiently than TfCel9A.

The tryptophan residues at positions 256, 209, and 313 in TfCel9A, which are involved in binding Glc-4, Glc-3, and Glc-2 of β-1,4-glucans, respectively, are missing in PttCel9A. To determine the effect of these residues on the substrate range of TfCel9A, the mutant enzymes W256S, W209A, and W313G were also screened on the polysaccharide substrates. Although the substrate range of TfCel9A and the mutant enzymes did not differ, the extent of hydrolysis by W313G was diminished.

Activity with Oligosaccharides. The shortest oligosaccharides hydrolyzed by the bacterial enzymes, TfCel9A and TfCel9B, were cellotetraose and cellotriose, respectively. TfCel9A consistently produced glucose upon hydrolysis of oligosaccharides and PASC. Since cellotetraose is the primary product of this enzyme on polymeric substrates, this is a consequence of further degradation of cellotetraose to cellotriose and glucose (*19*). TfCel9B produced glucose also through degradation of cellotriose to cellobiose and glucose. In contrast, only small amounts of glucose was produced by TfCel9B from cellotetraose, showing that the preferred mode of cleavage of this substrate is between two molecules of cellobiose. These results are consistent with the active site structures and modes of action of TfCel9A and TfCel9B (*19*, *31*). Notably, hydrolysis of PASC by TfCel9A yielded products no longer than cellotetraose, which is consistent with its unique processive endoglucanase activity (*32*).

As predicted from studies with polymeric substrates, hydrolysis of cellotetraose and shorter oligosaccharides by the plant enzyme Δ_{1-105}PttCel9A was not detected (Table 2). Δ_{1-105}PttCel9A showed low activity with cellopentaose and highest activity with cellohexaose. An inspection of the experimental (TfCel9A) and modeled (PttCel9A) structures of the enzyme active sites (Figure 2B) suggests that the loss of some of the key tryptophan residues that provide substrate binding interactions in the active site of the bacterial enzyme contributes to the low or no activity of PttCel9A on short oligosaccharides. The presence of 2−20 μM cellotetraose did not affect the rate of hydrolysis of CMC(4M) by Δ_{1-105}PttCel9A, and the presence of 200 μM to 2 mM cellotetraose did not affect the rate of hydrolysis of cellohexaose by Δ_{1-105}PttCel9A (data not shown). These results support the hypothesis that cellotetraose was not hydrolyzed by Δ_{1-105}PttCel9A due to inefficient substrate binding rather than inefficient hydrolysis of the compound. Glucose was not detected among the hydrolysis products from cellohexaose or PASC.

Δ_{1-105}PttCel9A, TfCel9A, nor TfCel9B released methylumbelliferone upon incubation with the MeUmb-cellooligosaccharides $MeUmbG_2$ through $MeUmbG_6$. The aromatic MeUmb group occupies substrate binding subsites of certain glycosyl hydrolases; however, the range of the chromogenic substrates hydrolyzed by Δ_{1-105}PttCel9A, TfCel9A, and TfCel9B could be correlated to the length of the oligosaccharide chain alone (Table 3). Although Δ_{1-105}PttCel9A hydrolyzed G5, hydrolysis of $MeUmbG_5$ was not detected. Furthermore, the major products from hydrolysis of cellohexaose by Δ_{1-105}PttCel9A were cellotetraose and cellobiose, whereas hydrolysis of $MeUmbG_6$ by Δ_{1-105}-PttCel9A yielded mainly cellotriose. The altered product distribution pattern observed for Δ_{1-105}PttCel9A may be partly explained by the MeUmb group interacting poorly with the protein and, thus, not being able to provide the necessary interactions for stabilization of a productive enzyme−substrate complex. In the case of $MeUmbG_6$, steric hindrance near the +2 subsite may prevent binding of the MeUmb moiety to the protein and force the oligosaccharide to bind in subsites +3 through −3, rather than +2 through −4, yielding cellotriose as the main product rather than cellotetraose and cellobiose. The lack of catalytic activity on $MeUmbG_5$ may then be explained by a nonproductive enzyme−substrate complex when subsite −3 is not occupied.

Kinetic Analyses with Cellohexaose. The specific activities of Δ_{1-105}PttCel9A, TfCel9A, and TfCel9B on 600 μM cellohexaose were 0.30 ± 0.07, 603 ± 57, and 52 ± 2 μmol mg^{-1} min^{-1}, respectively. The catalytic efficiency (k_{cat}/K_m) of Δ_{1-105}PttCel9A was approximately 3 orders of magnitude lower than the bacterial endoglucanases, TfCel9A and

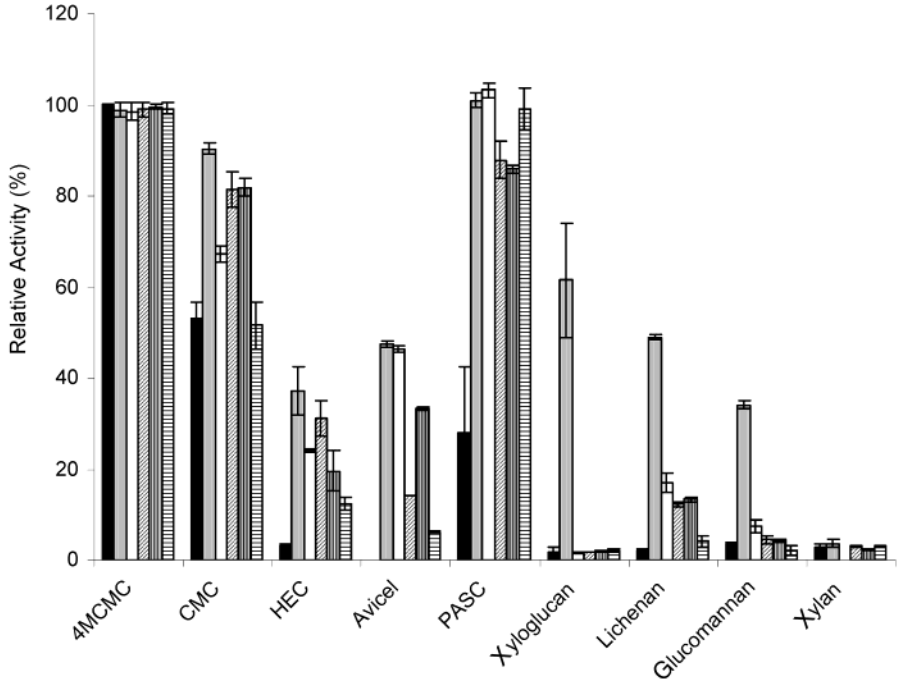

FIGURE 5: Substrate specifivity of Δ_{1-105}PttCel9A (black bars), TfCe9B (gray bars), TfCel9A (white bars), W256A (diagonal lines), W209S (vertical lines), and W313G (horizontal lines) on polymeric substrates. The substrate concentration in reaction mixtures was 0.1% (w/v). Exceptions were PASC (5%, w/v), glucomannan (0.01%), and lichenan (0.01%).

Table 2: Products Formed from Hydrolysis of Oligosaccharides from Cellobiose (G2) to Cellohexaose (G6) and PASC by PttCel9A, TfCel9B, and TfCel9A

		products[a] (%)					
enzyme	substrate	G1	G2	G3	G4	G5	G6
PttCel9A	cellobiose (G2)		100				
	cellotriose (G3)			100			
	cellotetraose (G4)				100		
	cellopentaose (G5)		15.3	25.9		58.8	
	cellohexaose (G6)		29.1	26.1	44.8		
	PASC		39.8	26.0	27.1	7.2	
TfCel9B	cellobiose		100				
	cellotriose	37.7	62.2				
	cellotetraose	1.8	98.2				
	cellopentaose	24.1	75.9				
	cellohexaose	11.1	88.9				
	PASC	1.5	97.7	0.8			
TfCel9A	cellobiose		100				
	cellotriose			100			
	cellotetraose	22.8	26.4	48.6	2.2		
	cellopentaose	32.2	24.8	43.0			
	cellohexaose	18.8	41.0	40.2			
	PASC	13.8	22.7	25.3	38.2		

[a] Reactions were performed in 50 mM K_2HPO_4 (pH 6.0) containing 250 μM substrate and 10 ng μL^{-1} enzyme and were incubated overnight at 30 °C. Products were analyzed by HPAEC-PAD using a CarboPac PA-100 column (Dionex).

Table 3: Products Formed from Hydrolysis of Methylumbelliferyl Oligosaccharides from $MeUmbG_2$ to $MeUmbG_6$ by PttCel9A, TfCel9B, and TfCel9A

		products[a] (%)					
enzyme	substrate	G1	G2	G3	G4	G5	G6
PttCel9A	$MeUmbG_2$	ND					
	$MeUmbG_3$	ND					
	$MeUmbG_4$	ND					
	$MeUmbG_5$	ND					
	$MeUmbG_6$			81.9	11.1		
TfCel9B	$MeUmbG_2$	ND					
	$MeUmbG_3$	1.7	98.3				
	$MeUmbG_4$	16.2	83.8				
	$MeUmbG_5$	8.9	91.1				
	$MeUmbG_6$	16.3	83.7				
TfCel9A	$MeUmbG_2$	ND					
	$MeUmbG_3$	ND					
	$MeUmbG_4$	6.8	9.7	83.5			
	$MeUmbG_5$	22.7	24.7	51.6	0.9		
	$MeUmbG_6$	26.8	25.8	45.6	1.7		

[a] Reactions were performed in 50 mM K_2HPO_4 (pH 6.0) containing 250 μM substrate and 10 ng μL^{-1} enzyme and were incubated overnight at 30 °C. Products were analyzed by HPAEC-PAD using a CarboPac PA-100 column (Dionex). Remaining substrate in reaction mixtures is not detected by the HPAEC−PAD system and so was not quantified. ND, not detected.

TfCel9B (Table 4). Although TfCel9B had the lowest K_m value, TfCel9A was twice as efficient as TfCel9B on cellohexaose. As indicated above, three tryptophan residues involved in substrate binding in TfCel9A are missing in PttCel9A. Tryptophan residues at subsites −4 and −3 in TfCel9A are also missing in TfCel9B (*20*). To determine how these tryptophan residues affect the efficiency of TfCel9A, steady-state kinetic parameters were also determined for W256A, W209S, and W313G.

The specific activities of mutants W256A, W209S, and W313G on 600 μM cellohexaose were 28 ± 3, 131 ± 11, and 7.4 ± 1 μmol mg^{-1} min^{-1}, respectively. Hydrolysis of cellohexaose by the mutant enzymes was less efficient than the wild-type enzyme, and mutation W313 to G had the most dramatic effect (Table 4). Particularly striking was the decrease in k_{cat} of W313G of more than 2 orders of magnitude. Cellotriose was produced by hydrolysis of cellohexaose by TfCel9A and W256S but not by W209A or W313G.

Kinetic Analyses with Cellotetraose. A correlation between aromatic amino acids at subsites −4, −3, and −2 and the ability to degrade short oligosaccharides was investigated by comparing the hydrolysis of cellotetraose by W256A,

Table 4: Steady-State Kinetic Parameters of Different Endoglucanases for Cellohexaose[a]

enzyme	k_{cat} (s^{-1})	K_m (μM)	k_{cat}/K_m	relative efficiency (%)
PttCel9A	2.3×10^{-2} (0.001)	1755 (673)	1.3×10^{-5} (5×10^{-6})	0.04
TfCel9B	1.3 (0.2)	97 (6)	1.4×10^{-2} (0.003)	39
TfCel9A	16.9 (2.0)	470 (27)	3.6×10^{-2} (0.002)	100
W209S	3.4 (0.6)	408 (50)	8.2×10^{-3} (0.0004)	23
W256A	1.1 (0.1)	921 (116)	1.2×10^{-3} (0.00002)	3
W313G	6.5×10^{-2} (0.002)	211 (19)	3.1×10^{-4} (0.00003)	0.9

[a] Reactions were performed in 50 mM K_2HPO_4 (pH 6.0) at 30 °C. Numbers in parentheses indicate standard deviation ($n = 3$).

W209S, W313G, and TfCel9A. The K_m values calculated for TfCel9A, W256A, and W313G exceeded 5 mM, whereas the K_m of W209S was 2.8 mM. Since the K_m values generally exceeded the maximum substrate concentration used in experiments, accurate determinations of k_{cat} and catalytic efficiency were not obtained. However, the specific activities of TfCel9A and the mutant enzymes W256A, W209S, and W313G on 600 μM cellotetraose were 0.28 ± 0.01, 1.1 ± 0.1, 0.29 ± 0.06, and 0.053 ± 0.007 μmol mg^{-1} min^{-1}, respectively. Thus, the specific activity of TfCel9A on cellotetraose was more than 3 orders of magnitude lower than that on cellohexaose. Furthermore, mutation of W313 to G consistently decreased the activity of TfCel9A, whereas mutation of W256 to A improved the specific activity of TfCel9A on cellotetraose.

DISCUSSION

To increase the potential of wood fibers as a raw material, the activities of carbohydrate-active enzymes involved in secondary cell wall synthesis can be targeted to modify cell wall composition. The membrane-bound endoglucanase, PttCel9A, is upregulated during secondary cell wall synthesis and is homologous to the *A. thaliana* enzyme, KOR (*4*). Proposed roles of KOR and homologous enzymes include (i) removing a possible precursor molecule from elongating cellulose chains (*33*), (ii) facilitating cellulose microfibril formation by excising amorphous cellulose (*13*), and (iii) regulating the length of cellulose chains in cellulose microfibrils (*13*). Korrigan-type plant cellulases might also hydrolyze amorphous regions of cellulose microfibrils to facilitate integration of other plant cell wall polymers. Thus, PttCel9A could be an effective target for fiber engineering. Here we report the recombinant expression and characterization of the catalytic domain of PttCel9A, Δ_{1-105}PttCel9A, and correlate its activity with its putative function in vivo.

It was necessary to screen a relatively large number of *P. pastoris* transformants before detecting a transformant that expressed Δ_{1-105}PttCel9A. Recombinant expression of the same protein in different *P. pastoris* transformants can vary significantly (*34*) and may result from multiple gene insertions. The gene fragment encoding Δ_{1-105}PttCel9A was PCR amplified from a positive *P. pastoris* transformant and sequenced to confirm that the successful expression of Δ_{1-105}PttCel9A by this transformant was not caused by a mutation. The expression of Δ_{1-105}PttCel9A in *P. pastoris* yielded higher amounts of the enzyme than the previously reported recombinant expression of the KOR homologue from *B. napus*, Δ_{1-90}Cel16 (*15*). In addition, the specific activity of Δ_{1-105}PttCel9A on CMC(4M) was more than 60 times higher than that of Δ_{1-90}Cel16 under the same conditions (*15*). Since PttCel9A and Cel16 share 82% sequence identity, the differences in their activities might reflect real differences in the native enzymes. However, it is also possible that, by reducing the temperature to 22 °C while inducing expression of Δ_{1-105}PttCel9A, more of active Δ_{1-105}PttCel9A was produced than for Δ_{1-90}Cel16 (*34*).

The comparatively narrow range of polysaccharides hydrolyzed by Δ_{1-105}PttCel9A was similar to the previous reports of Δ_{1-90}Cel16 activity (*15*). Like Δ_{1-90}Cel16, Δ_{1-105}PttCel9A efficiently hydrolyzed β-1,4-glucosyl linkages in CMC(4M), CMC, and PASC but not HEC, xyloglucan, or lichenan. The reducing end assay used in this study detects soluble oligosaccharides, and so the relative activity of Δ_{1-105}PttCel9A on PASC shown in Figure 5 may underestimate the true activity of this enzyme on amorphous cellulose. The substrate specificity of Δ_{1-105}PttCel9A is distinct from that of the two secreted GH9 enzymes from *P. calli*, PopCel1 and PopCel2, which hydrolyze xyloglucan and lichenan as well as CMC and PASC (*35*). PopCel1 and PopCel2 share less than 20% sequence identity with PttCe9A and have been implicated in cell wall expansion (*6*). The different substrate specificities of PttCel9A and the endoglucanases from *P. calli*, as well as their distinct regulatory patterns, reveal a diverse functionality for secreted and membrane-bound endoglucanases.

The broader substrate range of TfCel9A and TfCel9B, including their ability to hydrolyze shorter oligosaccharides than PttCel9A, is consistent with the different roles of bacterial and plant cellulases. Bacteria benefit from cellulases that have broad substrate specificity and high catalytic activity since bacterial cellulases provide cells with nutrients. In contrast, plant cellulases facilitate cell wall development, which would be hindered by excessive rates of cellulose hydrolysis. The present study shows that the active site of PttCel9A is designed to catalyze slow endolytic hydrolysis of cellulosic substrates with low crystallinity and a minimum DP of five to six glucose units. Such an activity is compatible with a function in releasing or editing growing cellulose chains, as has been proposed for other KOR homologues. However, mutations in PttCel9A that lead to modest increases in hydrolytic activity could impart beneficial properties to wood fibers, such as increased flexibility or altered cell shape. Our present data show that the low activity of PttCel9A can be correlated with the lack of some of the key tryptophans that provide substrate binding interactions in the related bacterial enzymes. Consequently, mutating, e.g., P439 (subsite −2) in PttCel9A to tryptophan could increase the activity of this enzyme toward cellulosic substrates. Although TfCel9B lacks a tryptophan that corresponds to W256 in TfCel9A, the crystal structures of GH9 enzymes from *C. cellulolyticum*, Cel9G and Cel9M, indicate that both W313 and W256 are conserved in these enzymes (*21*, *22*). Moreover, our data indicate that mutating W256 reduces the catalytic efficiency of TfCel9A on cellohexaose. Thus, mutating both P439 and G371 (subsite −4) in PttCel9A to tryptophan could additively increase the activity of this enzyme. W209 has been implicated in the processive activity of TfCel9A (*19*), and it is not conserved in TfCel9B, Cel9G,

or Cel9M, and mutating W209 affected TfCel9A activity less than mutating W256 or W313. If PttCel9A is involved in modifying elongating cellulose chains, then a gain in processive hydrolytic activity would likely be detrimental and T326 (subsite −3) should not be targeted.

Other molecular features in PttCel9A that can be targeted for fiber modification can be found by comparing the catalytic domains of plant GH9 enzymes that are membrane-anchored with those that are secreted. This comparison reveals several sequence characteristics that are unique to PttCel9A and membrane-anchored glycosyl hydrolases from *A. thaliana* (KOR, U37702; KOR2, AC001299; KOR3, AL078637), *B. napus* (Cel16, AJ242807), *Hordeum vulare* (cel1, AB040769), *Papaver somniferum* (BF010444), and *Lycopersicon esculentum* (cel3, U78526). Although several secreted enzymes lack a tryptophan residue corresponding to W313 (subsite −2) in TfCel9A, a substitution to proline (P439 in PttCel9A) is conserved among the membrane-anchored glycosyl hydrolases. The presence of the proline is likely to impose unique geometric constraints on the backbone at this position. The lack of an extended side chain may create a more open active site at the position of cleavage and provide altered possibilities for interactions with the substrate. The precise meaning of a conserved proline in this position is hard to assess in absence of mutagenesis, biochemical, and structural data. However, the loop in which P439 resides is longer in PttCel9A (residues 435−440) and korrigan-type glycosyl hydrolases than in GH9 enzymes that are not membrane-bound (residues 311−314 in TfCel9A). Moreover, the sequence is different, and it should be emphasized that, although the hydrophobic stacking interaction with the indole ring of Trp is missing in the membrane-bound enzymes, this stacking interaction may be replaced by a set of hydrogen bonds. Interestingly, our sequence comparison indicates that all of the secreted plant GH9 enzymes that contain C-terminal putative carbohydrate binding modules contain a tryptophan corresponding to W313 (subsite −2) in TfCel9A. If carbohydrate binding modules are retained by plant cellulases that require higher catalytic activity, then this correlation supports the prediction that substituting P439 to tryptophan in PttCel9A would increase the hydrolytic activity of this enzyme.

Compared to the secreted plant GH9 enzymes, sequence insertions, or loops, line the substrate binding cleft of PttCel9A and other korrigan-type glycosyl hydrolases. For example, a loop corresponding to the blocking loop in TfCel9A (residues 245−255; residues 359−369 in PttCel9A) is present in the membrane-anchored glycosyl hydrolases but is lacking in the secreted enzymes. Moreover, the sequence of the corresponding loop is highly conserved among the membrane-bound plant enzymes, while it is not conserved in soluble bacterial glycosyl hydrolases. This loop is likely to reflect the special requirements imposed by the unique function of PttCel9A and other KOR homologues. Indeed, a number of observations imply that this loop adopts a completely different conformation in the membrane-bound enzymes. First, a proline (P355 in PttCel9A) residue interrupts the α-helical segment that precedes this loop in GH9 enzymes. Second, two aromatic residues reside in this loop (F364 and W365), which might provide additional binding sites at the nonreducing end of an extended cellulose chain or, alternatively, interact with the microfibril structure. A second loop that is unique to the korrigan-type glycosyl hydrolases is situated at the reducing end of the binding cleft and is defined by residues 234−242 in PttCel9A. This loop is absent in other GH9 enzymes and appears in PttCel9A as an eight-residue insertion at a position immediately before the active site histidine (H125) in TfCel9A. This loop is expected to further delineate, and possibly extend, the substrate binding cleft toward the reducing end.

A proline-rich C-terminal sequence also appears to be a unique feature among catalytic domains of plant membrane-anchored glycosyl hydrolases. PttCel9A and other korrigan-type glycosyl hydrolases contain a unique C-terminal 16 residue long proline-rich motif following the catalytic core domain. Polyproline motifs are typically involved in protein−protein interactions (*36*), as well as other types of interactions, for instance, the interactions of polyphenols (tannins) with proline-rich motifs in the salivary proline-rich protein (*37*). Proline-rich motifs may also function in subcellular localization. Proline stretches tend to form polyproline II helices, which, by virtue of the unique characteristics of proline, provide extended and easily accessible hydrophobic interaction sites (often at the N- or C-terminus) referred to as "sticky arms" (*38*). Thus, there are several potential roles for the C-terminal poly(Pro) tail in plasma membrane-bound plant cellulases: (i) to guide the enzyme to the appropriate subcellular location, i.e., the plasma membrane; (ii) to promote transient association with carbohydrate moieties during microfibril trimming and processing at the cellulose deposition site of the secondary plant cell wall; or (iii) to provide a site for interaction with a yet unidentified protein partner.

The activity of PttCel9A reported in this study supports the proposed role for membrane-bound cellulases in cellulose microfibril assembly. Furthermore, we have identified features in the catalytic domain of these enzymes that may contribute to their substrate specificity and hydrolytic activity. Importantly, investigating the effect of selective mutations on the activity of PttCel9A will help to elucidate the role of this enzyme in vivo and could lead to the synthesis of wood fibers with novel and industrially relevant properties.

ACKNOWLEDGMENT

We thank Kathleen Piens for advice on oligosaccharide analysis, Harry Brumer for advice on mass spectral analysis, and Martin Bauman for optimizing the HPAEC-PAD system.

REFERENCES

1. Hertzberg, M., Aspeborg, H., Schrader, J., Andersson, A., Erlandsson, R., Blomqvist, K., Bhalerao, R., Uhlen, M., Teeri, T. T., Lundeberg, J., Sundberg, B., Nilsson, P., and Sandberg, G. (2001) A transcriptional road map to wood formation, *Proc. Natl. Acad. Sci. U.S.A. 98*, 14732−14737.
2. Sterky, F., Regan, S., Karlsson, J., Hertzberg, M., Rohde, A., Holmberg, A., Amini, B., Bhalerao, R., Larsson, M., Villarroel, R., Van Montagu, M., Sandberg, G., Olsson, O., Teeri, T. T., Boerjan, W., Gustafsson, P., Uhlen, M., Sundberg, B., and Lundeberg, J. (1998) Gene discovery in the wood-forming tissues of poplar: analysis of 5,692 expressed sequence tags, *Proc. Natl. Acad. Sci. U.S.A. 95*, 13330−13335.
3. Djerbi, S., Aspeborg, H., Nilsson, P., Mellerowicz, E., Sundberg, B., Blomqvist, K., and Teeri, T. T. (2003) Identification and expression analysis of wood specific cellulose synthase genes in hybrid aspen, *Cellulose* (in press).
4. Rudsander, U., Denman, S., Raza, S., and Teeri, T. T. (2003) Molecular features of family GH9 cellulases in hybrid aspen and

the filamentous fungus *Phanerochaete chrysosporium*, *J. Appl. Glycobiol. 50*, 253−256.
5. Ohmiya, Y., Samejima, M., Shiroishi, M., Amano, Y., Kanda, T., Sakai, F., and Hayashi, T. (2000) Evidence that endo-1,4-beta-glucanases act on cellulose in suspension-cultured poplar cells, *Plant J. 24*, 147−158.
6. Park, Y. W., Tominaga, R., Sugiyama, J., Furuta, Y., Tanimoto, E., Samejima, M., Sakai, F., and Hayashi, T. (2003) Enhancement of growth by expression of poplar cellulase in *Arabidopsis thaliana*, *Plant J. 33*, 1099−1106.
7. Nicol, F., His, I., Jauneau, A., Vernhettes, S., Canut, H., and Hofte, H. (1998) A plasma membrane-bound putative endo-1,4-beta-D-glucanase is required for normal wall assembly and cell elongation in *Arabidopsis*, *EMBO J. 17*, 5563−5576.
8. Lane, D. R., Wiedemeier, A., Peng, L. C., Hofte, H., Vernhettes, S., Desprez, T., Hocart, C. H., Birch, R. J., Baskin, T. I., Burn, J. E., Arioli, T., Betzner, A. S., and Williamson, R. E. (2001) Temperature-sensitive alleles of RSW2 link the KORRIGAN endo-1,4-beta-glucanase to cellulose synthesis and cytokinesis in *Arabidopsis*, *Plant Physiol. 126*, 278−288.
9. Sato, S., Kato, T., Kakegawa, K., Ishii, T., Liu, Y. G., Awano, T., Takabe, K., Nishiyama, Y., Kuga, S., Sato, S., Nakamura, Y., Tabata, S., and Shibata, D. (2001) Role of the putative membrane-bound endo-1,4-beta-glucanase KORRIGAN in cell elongation and cellulose synthesis in *Arabidopsis thaliana*, *Plant Cell Physiol. 42*, 251−263.
10. Szyjanowicz, P. M. J., McKinnon, I., Taylor, N. G., Gardiner, J., Jarvis, M. C., and Turner, S. R. (2004) The irregular xylem 2 mutant is an allele of korrigan that affects the secondary cell wall of *Arabidopsis thaliana*, *Plant J. 37*, 730−740.
11. Zuo, J. R., Niu, Q. W., Nishizawa, N., Wu, Y., Kost, B., and Chua, N. H. (2000) KORRIGAN, an *Arabidopsis* endo-1,4-beta-glucanase, localizes to the cell plate by polarized targeting and is essential for cytokinesis, *Plant Cell 12*, 1137−1152.
12. Brummell, D. A., Catala, C., Lashbrook, C. C., and Bennett, A. B. (1997) A membrane-anchored E-type endo-1,4-beta-glucanase is localized on Golgi and plasma membranes of higher plants, *Proc. Natl. Acad. Sci. U.S.A. 94*, 4794−4799.
13. Molhoj, M., Pagant, S. R., and Hofte, H. (2002) Towards understanding the role of membrane-bound endo-beta-1,4-glucanases in cellulose biosynthesis, *Plant Cell Physiol. 43*, 1399−1406.
14. Silva-Filho, M. C. (2003) One ticket for multiple destinations: dual targeting of proteins to distinct subcellular locations, *Curr. Opin. Plant Biol. 6*, 589−595.
15. Molhoj, M., Ulvskov, P., and Dal Degan F. (2001) Characterization of a functional soluble form of a *Brassica napus* membrane-anchored endo-1,4-beta-glucanase heterologously expressed in *Pichia pastoris*, *Plant Physiol. 127*, 674−684.
16. Ross, P., Mayer, R., and Benziman, M. (1991) Cellulose biosynthesis and function in bacteria, *Microbiol. Rev. 55*, 35−58.
17. Matthysse, A. G., Thomas, D. L., and White, A. R. (1995) Mechanism of cellulose synthesis in *Agrobacterium tumefaciens*, *J. Bacteriol. 177*, 1076−1081.
18. Matthysse, A. G., White, S., and Lightfoot, R. (1995) Genes required for cellulose synthesis in *Agrobacterium tumefaciens*, *J. Bacteriol. 177*, 1069−1075.
19. Sakon, J., Irwin, D., Wilson, D. B., and Karplus, P. A. (1997) Structure and mechanism of endo/exocellulase E4 from *Thermomonospora fusca*, *Nat. Struct. Biol. 4*, 810−818.
20. Lin, E., and Wilson, D. B. (1988) Identification of a CelE-binding protein and its potential role in induction of the c*elE* gene in *Thermomonospora fusca*, *J. Bacteriol. 170*, 3843−3846.
21. Parsiegla, G., Belaich, A., Belaich, J. P., and Haser, R. (2002) Crystal structure of the cellulase Ce19M enlightens structure/function relationships of the variable catalytic modules in glycoside hydrolases, *Biochemistry 41*, 11134−11142.
22. Mandelman, D., Belaich, A., Belaich, J. P., Aghajari, N., Driguez, H., and Haser, R. (2003) X-ray crystal structure of the multidomain endoglucanase Cel9G from *Clostridium cellulolyticum* complexed with natural and synthetic cello-oligosaccharides, *J. Bacteriol. 185*, 4127−4135.
23. Ausubel, F., Brent, R., Kingston, R. E., Moore, D. D., Seidman, J. G., Smith, J. A., and Struhl, K. (1999) *Current Protocols in Molecular Biology*, John Wiley & Sons, New York.
24. Morrissey, J. H. (1981) Silver stain for proteins in polyacrylamide gels—a modified procedure with enhanced uniform sensitivity, *Anal. Biochem. 117*, 307−310.
25. Rosenfeld, J., Capdevielle, J., Guillemot, J. C., and Ferrara, P. (1992) In-gel digestion of proteins for internal sequence-analysis after 1-dimensional or 2-dimensional gel-electrophoresis, *Anal. Biochem. 203*, 173−179.
26. Hellman, U., Wernstedt, C., Gonez, J., and Heldin, C. H. (1995) Improvement of an in-gel digestion procedure for the micropreparation of internal protein-fragments for amino acid sequencing, *Anal. Biochem. 224*, 451−455.
27. Zhang, S., Lao, G. F., and Wilson, D. B. (1995) Characterization of a *Thermomonospora fusca* exocellulase, *Biochemistry 34*, 3386−3395.
28. Jones, T. A., Zou, J.-Y., Cowan, S. W., and Kjeldgaard, M. (1991) Improved methods for building protein models in electron density maps and the location of errors in these models, *Acta Crystallogr., Sect. A 47*, 110−119.
29. Brünger, A. T., Adams, P. D., Clore, G. M., DeLano, W. L., Gros, P., Grosse-Kunstleve, R. W., Jiang, J.-S., Kuszewski, J., Nilges, M., Pannu, N. S., Read, R. J., Rice, L. M., Simonson, T., and Warren, G. L. (1998) Crystallography & NMR system: a new software suite for macromolecular structure determination, *Acta Crystallogr., Sect. D 54*, 905−921.
30. Garcia, E., Johnston, D., Whitaker, J. R., and Shoemaker, S. P. (1993) Assessment of endo-1,4-beta-D-glucanase activity by a rapid colorimetric assay using disodium 2,2′-bicinchoninate, *J. Food Biochem. 17*, 135−145.
31. Irwin, D. C., Spezio, M., Walker, L. P., and Wilson, D. B. (1993) Activity studies of 8 purified cellulases—specificity, synergism, and binding domain effects, *Biotechnol. Bioeng. 42*, 1002−1013.
32. Barr, B. K., Hsieh, Y. L., Ganem, B., and Wilson, D. B. (1996) Identification of two functionally different classes of exocellulases, *Biochemistry 35*, 586−592.
33. Peng, L. C., Kawagoe, Y., Hogan, P., and Delmer, D. (2002) Sitosterol-beta-glucoside as primer for cellulose synthesis in plants, *Science 295*, 147−150.
34. Bencurova, M., Rendic, D., Fabini, G., Kopecky, E. M., Altmann, F., and Wilson, I. B. H. (2003) Expression of eukaryotic glycosyltransferases in the yeast *Pichia pastoris*, *Biochimie 85*, 413−422.
35. Nakamura, S., and Hayashi, T. (1993) Purification and properties of an extracellular endo-1,4-beta-glucanase from suspension-cultured Poplar cells, *Plant Cell Physiol. 34*, 1009−1013.
36. Kay, B. K., Williamson, M. P., and Sudol, M. (2000) The importance of being proline: the interaction of proline-rich motifs in signaling proteins with their cognate domains, *FASEB J. 14*, 231−241.
37. Baxter, N. J., Lilley, T. H., Haslam, E., and Williamson, M. P. (1997) Multiple interactions between polyphenols and a salivary proline-rich protein repeat result in complexation and precipitation, *Biochemistry 36*, 5566−5577.
38. Williamson, M. P. (1994) The structure and function of proline-rich regions in proteins, *Biochem. J. 297*, 249−260.
39. DeLano, W. L. (2002) *The PyMOL user's manual*, DeLano Scientific, San Carlos, CA.

BI049453X